

In-Flight Inertia Matrix Estimation of a Gyroless Satellite

C. Nainer, H. Garnier, M. Gilson, H. Evain and C. Pittet

Abstract Knowledge of the inertia parameters is vital to guarantee a correct attitude control of a spacecraft. The relatively low accuracy of their estimate prior to launch, together with possible changes of these quantities, make the in-orbit inertia estimation a problem of great interest. In this work, the estimation of the inertia matrix for a gyroless satellite is considered. An iterative instrumental variable algorithm is proposed that relies on the star tracker measurements. A semi-adaptive filter is designed in order to achieve low variance estimates, by taking care of both sensor noise and torque disturbances. The performance of the proposed algorithm is then analyzed via Monte Carlo simulations, using data generated from a high-fidelity simulator.

Carlo Nainer
Université de Lorraine, CNRS, CRAN, F-54000 Nancy, France, and CNES F-31401 Toulouse, France
e-mail: carlo.nainer@univ-lorraine.fr

Hugues Garnier
Université de Lorraine, CNRS, CRAN, F-54000 Nancy, France,
e-mail: hugues.garnier@univ-lorraine.fr

Marion Gilson
Université de Lorraine, CNRS, CRAN, F-54000 Nancy, France,
e-mail: marion.gilson@univ-lorraine.fr

Hélène Evain
CNES F-31401 Toulouse, France,
e-mail: helene.evain@cnes.fr

Christelle Pittet
CNES F-31401 Toulouse, France,
e-mail: christelle.pittet@cnes.fr

1 Introduction

Accurate mathematical models of satellite dynamics are essential for the validation of control algorithms. The mass distribution is the most important parameter that governs the spacecraft dynamics, and its knowledge is used to build high fidelity simulators that are later used to test new control laws. However, the satellite inertia cannot be accurately estimated prior to launch: the estimates from computer-aided design (CAD) software usually present errors up to 10%; moreover, the mass distribution may change after launch due to some activities such as fuel consumption and deployment of solar panels. For these reasons, a precise in-flight estimation of the satellite inertia parameters has a great importance.

Several works considered the inertia estimation problem. Different methods were used for the estimation: simple least squares approach (e.g. [1]), extended Kalman filter (e.g. [2]), joint-dual unscented Kalman filter [3], constrained least-squares rewritten into semidefinite programming form [4], maximum likelihood method [5]. The majority of these works considered satellites equipped with a gyroscope, and therefore the angular rate measurement were directly obtained by this instrument. However, small satellites (Myriade [6], CubeSats, ...) are emerging due to their lower cost. These types of satellites have less sensor availability compared to bigger spacecraft, making the attitude determination as well as parameter estimation more challenging. Usually in larger satellites, both star tracker and accurate gyroscope (e.g. fiber-optic gyroscopes (FOG)) are used for attitude and rate estimation. However, in smaller satellites, for size or cost constraints only small MEMS gyroscopes are used. These gyroscopes present much worse accuracy than FOGs, due to much higher random walk noise and to an higher sensitivity to the environment conditions. These type of satellites rely only on star tracker measurements for both attitude and rate estimation. Studies on attitude and rate estimation in gyroless conditions have been made, however, few studies focused on the satellite parameter estimation from star tracker measurements only. In [7] the authors proposed an attitude parameter-calibration Kalman filter (APKF) that only uses star tracker measurements as well as reaction wheel speed reading. Beside the attitude and rate estimation, the spacecraft inertia, as well as the sensor misalignment and residual dipole moment were identified.

In this paper, we propose an instrumental variable (IV) approach to estimate the satellite inertia without relying on rate sensors. The input-output data used for the estimation are only the reaction wheel speed readings and the star tracker measurements. One of the reason behind the choice of the IV method consists in its robustness with respect to the initial conditions (due to its convex cost function) and to the user-parameters.

The paper is structured as follows. Section 2 describes the satellite closed-loop system. In Section 3, the satellite modeling and the IV approach are described. This estimation method includes a sub-optimal filtering to improve the identification performance by a significant reduction of the estimation variance. Finally, in Section 4 the performance of the proposed algorithm, tested through Monte Carlo simulations in a high-fidelity simulator of the satellite Microcarb, is illustrated.

2 Satellite system

2.1 Satellite Closed-Loop System

For this study we consider the Microcarb satellite. Microcarb is a micro-satellite that will be launched in 2021 to map sources and sinks of carbon dioxide. Since the satellite dynamics is unstable (it contains two integrators from torque to attitude), all the experiments must be carried out under a closed-loop control configuration. The overall system is shown in Figure 1. Since the spacecraft is gyroless, and to improve the signal to noise ratio, the feedback includes an extended Kalman filter (EKF) that estimates the satellite angular rate (required by the controller) from the attitude measurements (e.g. [8]). The satellite controller structure [9] is as follows

$$K(s) = (K_p + K_d \cdot s) \frac{1}{s} \frac{1}{1 + \tau_1 \cdot s} \frac{1 + \tau_2 \cdot s}{1 + \tau_3 \cdot s}, \quad (1)$$

and it includes the following feedforward control law

$$K_{ff} = G_{ff} \cdot J_{sat} \cdot \dot{\omega}_{target}(t + \Delta T), \quad (2)$$

where J_{sat} is the satellite inertia, $\dot{\omega}_{target}$ is the target acceleration, G_{ff} and ΔT are two tuning parameters.

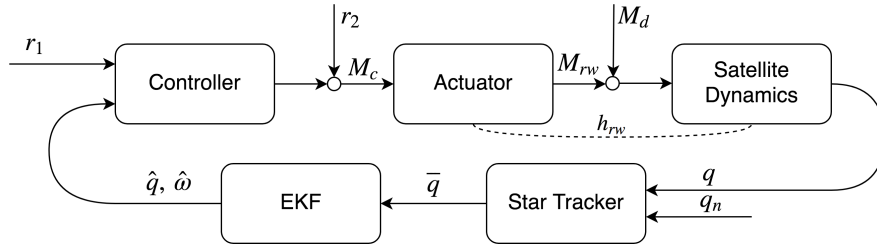


Fig. 1: Closed-loop satellite system. The equivalent torque generated by the reaction wheels is represented by M_{rw} , while r_1 and r_2 are the reference and feedforward signals, respectively.

2.2 Satellite Dynamic Model

The rotational dynamics of a rigid body, expressed in the satellite body frame, can be described by the Euler's equations (e.g. [10])

$$M(t) = J\dot{\omega}(t) + \omega(t) \wedge J\omega(t), \quad (3)$$

with $M(t) \in \mathbb{R}^{3 \times 1}$ is the sum of the applied torques, $J \in \mathbb{R}^{3 \times 3}$ is the inertia matrix, $\omega(t) \in \mathbb{R}^{3 \times 1}$ is the satellite angular rate in the body reference frame, and \wedge is the cross product operator, where all these variables and parameters are expressed in the body reference frame. The inertia matrix J has the following form

$$J = \begin{bmatrix} J_{11} & J_{12} & J_{13} \\ J_{12} & J_{22} & J_{23} \\ J_{13} & J_{23} & J_{33} \end{bmatrix}, \quad (4)$$

and the following properties

- J is symmetric (as shown in (4));
- J is positive definite;
- the diagonal terms of J are constrained by the triangle inequality:

$$J_{ii} < J_{jj} + J_{kk} \quad \forall \quad i \neq j \neq k. \quad (5)$$

The cross product multiplication $\omega(t) \wedge J\omega(t)$ in (3) can be rewritten as

$$\omega(t)^\times J\omega(t), \quad (6)$$

where

$$\omega(t)^\times = \begin{bmatrix} 0 & -\omega_3(t) & \omega_2(t) \\ \omega_3(t) & 0 & -\omega_1(t) \\ -\omega_2(t) & \omega_1(t) & 0 \end{bmatrix}. \quad (7)$$

For a satellite equipped with reaction wheels, the dynamics can be described as follows

$$-\dot{h}_{rw}(t) - \omega(t)^\times h_{rw}(t) + M_d(t) = J\dot{\omega}(t) + \omega(t)^\times J\omega(t), \quad (8)$$

where h_{rw} is the reaction wheel total angular momentum, and $M_d(t)$ is the sum of the disturbance torques applied to the spacecraft. The total disturbance torque depends on several factors: gravity gradient torque, aerodynamic torque, solar radiation pressure, magnetic torque, as well as internal oscillation in the satellite structure (the satellite is not a rigid body, having flexible elements like the solar panels). A detailed description of the disturbances is out of the scope of this paper. The reader may refer to the specific literature (e.g [10]) for further details. The total reaction wheel angular momentum is defined as follows

$$h_{rw}(t) = \sum_{i=1}^N J_{rw,i} \Omega_i(t) a_i, \quad (9)$$

where $\Omega_i(t)$ is the i -th reaction wheel speed, $J_{rw,i}$ is the i -th reaction wheel inertia (around its spinning axis), and a_i is the i -th reaction wheel orientation (in the satellite reference frame) expressed as a unit vector. In this study the reaction wheel alignments are considered to be exactly known, therefore their estimation is not required.

2.3 Attitude Representation

Quaternions are commonly used for the satellite attitude representation, since they do not present any singular configuration, at the contrary of the Euler's angle representation (e.g. [11]). In this paper, the following notation is used for the quaternions

$$q = [q_0, q_1, q_2, q_3]^T = \begin{bmatrix} q_0 \\ q_{1:3} \end{bmatrix}, \quad (10)$$

where q_0 and $q_{1:3}$ are the scalar and imaginary part, respectively. Details about the quaternion properties can be found in literature (e.g. [11]). The quaternions describing the body's attitude can be directly related to the angular velocity ($\omega \in \mathbb{R}^{3 \times 1}$) and its derivative in the body reference frame

$$\omega = 2W(q)\dot{q}, \quad \dot{\omega} = 2W(q)\ddot{q} \quad (11)$$

where \dot{q} and \ddot{q} are the quaternion derivatives, and $W(\cdot)$ is defined as follows

$$W(q) = \begin{bmatrix} q_1 & q_0 & q_3 & -q_2 \\ -q_2 & -q_3 & q_0 & q_1 \\ -q_3 & q_2 & -q_1 & q_0 \end{bmatrix}. \quad (12)$$

2.4 Sensors

2.4.1 Reaction wheel sensor

The reaction wheels are usually equipped with Hall-effect sensors or optical encoders in order to measure their angular speed Ω_i . The speed derivatives, $\dot{\Omega}_i$, are usually computed as a simple numerical differentiation, since these types of sensor are very accurate. We could assume the readings of Ω_i affected by a white noise, however since angular encoders are usually more accurate than other sensors (e.g. star tracker), for simplicity we consider these measurements noise free in this study.

2.4.2 Star Tracker

A star tracker provides the attitude measurements from the reference inertial frame to the satellite sensor frame. Its measurement equation can be described as follows

$$\bar{q} = q_n \otimes q_s \otimes q \quad (13)$$

where \otimes represents the quaternion multiplication operator (e.g [11]), \bar{q} is the measured quaternion, q_s is the quaternion representing the rotation from the body frame to the sensor frame (sensor alignment), q is the noise-free quaternion representing

the satellite attitude, and q_n is the quaternion noise that can be approximated as

$$q_n \simeq \begin{bmatrix} 1 \\ e_x/2 \\ e_y/2 \\ e_z/2 \end{bmatrix}, \quad (14)$$

with

$$e_x \sim N(0, \sigma_x^2), \quad e_y \sim N(0, \sigma_y^2), \quad e_z \sim N(0, \sigma_z^2) \quad (15)$$

where the three noise components, e_x, e_y, e_z , are considered mutually uncorrelated. More accurate star tracker models may include also a misalignment/bias term. In this study, we assume that the sensor alignment (q_s) is perfectly known, however, in the simulations, a small bias term is introduced in the star tracker sensor.

2.4.3 Noise on the Angular Rate Computed from the Quaternions

Let us start by considering the case where the star tracker is aligned with the body reference frame. The measurement equation (13) becomes

$$\bar{q} = q_n \otimes q, \quad (16)$$

where, from assumption (14), and by expanding (16) we obtain

$$\bar{q} = \begin{bmatrix} q_0 - \frac{e_x q_1}{2} - \frac{e_y q_2}{2} - \frac{e_z q_3}{2} \\ q_1 + \frac{e_x q_0}{2} - \frac{e_y q_3}{2} + \frac{e_z q_2}{2} \\ q_2 + \frac{e_x q_3}{2} + \frac{e_y q_0}{2} - \frac{e_z q_1}{2} \\ q_3 - \frac{e_x q_2}{2} + \frac{e_y q_1}{2} + \frac{e_z q_0}{2} \end{bmatrix}, \quad (17)$$

therefore the measured quaternion can be rewritten as

$$\bar{q} = q + \tilde{q}, \quad (18)$$

where

$$\tilde{q} = \begin{bmatrix} -\frac{e_x q_1}{2} - \frac{e_y q_2}{2} - \frac{e_z q_3}{2} \\ \frac{e_x q_0}{2} - \frac{e_y q_3}{2} + \frac{e_z q_2}{2} \\ \frac{e_x q_3}{2} + \frac{e_y q_0}{2} - \frac{e_z q_1}{2} \\ -\frac{e_x q_2}{2} + \frac{e_y q_1}{2} + \frac{e_z q_0}{2} \end{bmatrix}. \quad (19)$$

From (11) the angular rate $\bar{\omega}$ can be computed from the measured quaternions (and their derivatives)

$$\bar{\omega} = 2W(\bar{q})\dot{\bar{q}} = 2W(q)\dot{q} + 2W(\tilde{q})\dot{q} + 2W(q)\dot{\tilde{q}} + 2W(\tilde{q})\dot{\tilde{q}}, \quad (20)$$

with

$$\dot{\tilde{q}} = \frac{1}{2} \begin{bmatrix} -\dot{e}_x q_1 - e_x \dot{q}_1 - \dot{e}_y q_2 - e_y \dot{q}_2 - \dot{e}_z q_3 - e_z \dot{q}_3 \\ \dot{e}_x q_0 - e_x \dot{q}_0 - \dot{e}_y q_3 - e_y \dot{q}_3 + \dot{e}_z q_2 + e_z \dot{q}_2 \\ -\dot{e}_x q_3 - e_x \dot{q}_3 + \dot{e}_y q_0 + e_y \dot{q}_0 - \dot{e}_z q_1 - e_z \dot{q}_1 \\ -\dot{e}_x q_2 - e_x \dot{q}_2 + \dot{e}_y q_1 + e_y \dot{q}_1 + \dot{e}_z q_0 + e_z \dot{q}_0 \end{bmatrix}. \quad (21)$$

and where \dot{e}_i represents the numerical differentiation of e_i , and therefore having as variance $\sigma_{\dot{e}_i}^2 = 2\sigma_{e_i}^2/(\Delta T)^2$ (or $\sigma_{\dot{e}_i}^2 = 2\sigma_{e_i}^2/(2\Delta T)^2$ in case of the central differentiation) where ΔT is the sampling period.

Equation (21) can be approximated as

$$\dot{\tilde{q}} \simeq \frac{1}{2} \begin{bmatrix} -\dot{e}_x q_1 - \dot{e}_y q_2 - \dot{e}_z q_3 \\ \dot{e}_x q_0 - \dot{e}_y q_3 + \dot{e}_z q_2 \\ -\dot{e}_x q_3 + \dot{e}_y q_0 - \dot{e}_z q_1 \\ -\dot{e}_x q_2 + \dot{e}_y q_1 + \dot{e}_z q_0 \end{bmatrix}, \quad (22)$$

assuming

$$\dot{e} q \gg e \dot{q}, \quad (23)$$

which is a very realistic condition in our satellite scenario.

Since $2W(q)\dot{q} = \omega$, the noise on $\bar{\omega}$ is as follows

$$\tilde{\omega} = \bar{\omega} - \omega = 2W(\tilde{q})\dot{q} + 2W(q)\dot{\tilde{q}} + 2W(\tilde{q})\dot{\tilde{q}}. \quad (24)$$

From assumption (23), and considering that $q \gg \tilde{q}$, the overall noise on the angular rate can be approximated as

$$\tilde{\omega} \simeq 2W(q)\dot{\tilde{q}} = \begin{bmatrix} \dot{e}_x(q_0^2 + q_1^2 + q_2^2 + q_3^2) \\ \dot{e}_y(q_0^2 + q_1^2 + q_2^2 + q_3^2) \\ \dot{e}_z(q_0^2 + q_1^2 + q_2^2 + q_3^2) \end{bmatrix} = \begin{bmatrix} \dot{e}_x \\ \dot{e}_y \\ \dot{e}_z \end{bmatrix}, \quad (25)$$

since $q(t)$ is a unit quaternion.

From this result, the overall noise on the angular rate is directly related to the noise on the quaternions, and if the noise e is zero-mean and with components mutually uncorrelated, the same can be said for $\tilde{\omega}$.

In the more general case where the star tracker is not aligned with the body reference frame, an additional rotation must be performed. Therefore the angular rate ω in the satellite frame can be written as

$$\omega = R \omega_{st}, \quad (26)$$

where ω_{st} is the angular rate in the star tracker reference frame and R is the rotation matrix moving from the star tracker to the body reference frame. If the three components of the noise e have the same standard deviation σ_e then, even after the rotation the noise term $\tilde{\omega}$ remains zero-mean with its three components mutually uncorrelated. However, if the three noise components have different variance, then there will be a correlation between $\tilde{\omega}_x$, $\tilde{\omega}_y$ and $\tilde{\omega}_z$.

3 Satellite Inertia Estimation

3.1 Satellite Model in Linear Regression Form

Equation (8) can be rewritten in linear regression form as

$$-\dot{h}_{rw} - \omega^\times h_{rw} + M_d = \left(\Gamma(\dot{\omega}) + \omega^\times \Gamma(\omega) \right) \theta. \quad (27)$$

where $\theta = [J_{11}, J_{22}, J_{33}, J_{23}, J_{13}, J_{12}]^T$ and, given a vector $x = [x_1, x_2, x_3]^T$, the operator $\Gamma(\cdot)$ is defined as follows

$$\Gamma(x) = \begin{bmatrix} x_1 & 0 & 0 & 0 & x_3 & x_2 \\ 0 & x_2 & 0 & x_3 & 0 & x_1 \\ 0 & 0 & x_3 & x_2 & x_1 & 0 \end{bmatrix}. \quad (28)$$

3.1.1 Noise Term in the Linear Regression Model

The overall effect of the noise must be studied on the full dynamic model. Considering the equation

$$\bar{\omega} = \omega + \tilde{\omega}, \quad (29)$$

where ω is the noise-free satellite angular rate, the system in linear regression form can be rewritten as

$$-\dot{h}_{rw} - (\bar{\omega} - \tilde{\omega})^\times h_{rw} + M_d = \left(\Gamma(\dot{\bar{\omega}} - \dot{\tilde{\omega}}) + (\bar{\omega} - \tilde{\omega})^\times \Gamma(\bar{\omega} - \tilde{\omega}) \right) \theta, \quad (30)$$

or to keep the notation simpler

$$-\dot{h}_{rw} - (\bar{\omega} - \tilde{\omega})^\times h_{rw} + M_d = \phi^T(\dot{\omega}, \omega) \theta. \quad (31)$$

Following the approach shown in [12], the regressor matrix ϕ can be split into three terms

$$\phi = \psi - \delta - \varepsilon, \quad (32)$$

where

$$\psi^T = \Gamma(\dot{\bar{\omega}}) + \bar{\omega}^\times \Gamma(\bar{\omega}), \quad (33)$$

$$\delta^T = \Gamma(\dot{\tilde{\omega}}) + \tilde{\omega}^\times \Gamma(\tilde{\omega}), \quad (34)$$

$$\varepsilon^T = \omega^\times \Gamma(\tilde{\omega}) + \tilde{\omega}^\times \Gamma(\omega). \quad (35)$$

The overall system equation can be rewritten as

$$-\dot{h}_{rw} - \bar{\omega}^\times h_{rw} = \psi^T(\bar{\omega}, \bar{\omega}) \theta + v - M_d, \quad (36)$$

where $v = -\delta^T \theta - \varepsilon^T \theta - \bar{\omega}^\times h_{rw}$. The noise term $\bar{\omega}$ appears in a quadratic form only in the second term of (34) as

$$\begin{bmatrix} 0 & -\tilde{\omega}_2 \tilde{\omega}_3 & \tilde{\omega}_2 \tilde{\omega}_3 & (\tilde{\omega}_2^2 - \tilde{\omega}_3^2) & \tilde{\omega}_1 \tilde{\omega}_2 & -\tilde{\omega}_1 \tilde{\omega}_3 \\ \tilde{\omega}_1 \tilde{\omega}_3 & 0 & -\tilde{\omega}_1 \tilde{\omega}_3 & -\tilde{\omega}_1 \tilde{\omega}_2 & (\tilde{\omega}_3^2 - \tilde{\omega}_1^2) & \tilde{\omega}_2 \tilde{\omega}_3 \\ -\tilde{\omega}_1 \tilde{\omega}_2 & \tilde{\omega}_1 \tilde{\omega}_2 & 0 & \tilde{\omega}_1 \tilde{\omega}_3 & -\tilde{\omega}_2 \tilde{\omega}_3 & (\tilde{\omega}_1^2 - \tilde{\omega}_2^2) \end{bmatrix}. \quad (37)$$

Even if the noise term e is assumed to be zero-mean (15), the overall noise v may have non-zero expected value due to its nonlinear terms (37). Only if $\sigma_x = \sigma_y = \sigma_z$ (and $\tilde{\omega}_1, \tilde{\omega}_2, \tilde{\omega}_3$ are mutually uncorrelated) the nonlinear noise terms (37) are overall still zero-mean. Otherwise, if each axis presents a different noise standard deviation (common for star trackers), then $E(v) \neq 0$, where $E(\cdot)$ is the expectation operator.

From now on, we will consider the regressor $\psi^T(\cdot)$ directly as function of the quaternions and their derivatives

$$\psi^T(\bar{q}(t), \dot{\bar{q}}(t), \ddot{\bar{q}}(t)) = \Gamma(2W(\bar{q}(t))\ddot{\bar{q}}(t)) + (2W(\bar{q}(t))\dot{\bar{q}}(t))^\times \Gamma(2W(\bar{q}(t))\dot{\bar{q}}(t)), \quad (38)$$

and therefore the overall model in linear regression form becomes

$$-\dot{h}_{rw}(t) - (2W(\bar{q}(t))\dot{\bar{q}}(t))^\times h_{rw}(t) = \psi^T(\bar{q}(t), \dot{\bar{q}}(t), \ddot{\bar{q}}(t)) \theta + v(t) - M_d(t). \quad (39)$$

3.2 Derivative Estimates

The model (39) is function of the attitude quaternion $q(t)$, as well of its derivatives $\dot{q}(t)$, $\ddot{q}(t)$. However the star tracker provides only the angular position \bar{q} . The simplest solution would be to perform a numerical differentiation, having as main drawback a significant noise amplification. A way to limit the noise amplification consists in filtering the signal before performing the differentiation. The filter should not create any phase lag, therefore a smoothing operation based on a Butterworth low-pass filter has been used, where the filter is applied on both directions in order to cancel any phase lag inherent in the simple filtering. The filter cut-off frequency must be chosen larger than the noise-free signal bandwidth in order to avoid any distortion.

3.3 Instrumental Variable Method for Inertia Parameter Estimate

For this work, an instrumental variable (IV) method has been chosen for the estimation of the inertia parameters from the telemetry data. The IV method has been studied for several years since it is able to overcome some of the limitations of the

least square method while retaining its simplicity (e.g. [13] and [14]). Several form of IV algorithms have been developed, with the principal objective of achieving the smallest variance of the estimate, like the refined IV (e.g. [15]). The IV method was applied recently for a similar, but simpler (presence of gyroscope and ideal spacecraft dynamics), satellite estimation problem in [16].

The main reasons behind the choice of an IV approach are the following: it can be applied to a linear regression form model (with respect to the parameters) independently whether the states appear linearly; it relies on a convex cost function with an analytical solution; it is able to overcome the least squares limitation regarding the consistency of the estimates; since the system presents “mild” nonlinearities (at the typical satellite angular rate the gyroscopic term has a minor impact compared to the linear term), approximate optimal filtering can be applied (and therefore it can achieve estimates close to minimum variance).

3.3.1 Instrumental Variable Method

Given the model in linear regression form

$$M_{rw}(t) = \psi^T \left(\bar{q}(t), \dot{\bar{q}}(t), \ddot{\bar{q}}(t) \right) \theta + v(t) - M_d(t), \quad (40)$$

where $M_{rw}(t) = -\dot{h}_{rw}(t) - (2W(\bar{q}(t))\dot{\bar{q}}(t)) \times h_{rw}(t)$, the IV solution consists in the minimization of the following cost function

$$\hat{\theta}_{IV} = \arg \min_{\theta} \sum_{k=1}^N \left\| Z(t_k) \left(M_{rw}(t_k) - \psi^T(t_k) \theta \right) \right\|^2, \quad (41)$$

with N being the number of samples, and where the “instrument” Z^T has to respect the following properties in order to guarantee consistent estimates:

$$\begin{cases} \bar{E}(Z\psi^T) \text{ is non singular} \\ \bar{E}(Zv) = 0 \end{cases} \quad (42)$$

where $\bar{E}(\cdot) = \lim_{N \rightarrow \infty} \frac{1}{N} \sum_{k=1}^N E(\cdot)$. The IV method has an analytical solution closely related to the least squares one (e.g. [14])

$$\hat{\theta}_{IV} = \left[\sum_{k=1}^N Z(t_k) \psi^T(t_k) \right]^{-1} \left[\sum_{k=1}^N Z(t_k) M_{rw}(t_k) \right], \quad (43)$$

or more simply as

$$\hat{\theta}_{IV} = (Z\psi^T)^{-1}(ZM_{rw}), \quad (44)$$

where

$$\boldsymbol{\psi}^T = \begin{bmatrix} \boldsymbol{\psi}^T(t_1) \\ \boldsymbol{\psi}^T(t_2) \\ \vdots \\ \boldsymbol{\psi}^T(t_N) \end{bmatrix}, \quad \mathbf{Z}^T = \begin{bmatrix} \mathbf{Z}^T(t_1) \\ \mathbf{Z}^T(t_2) \\ \vdots \\ \mathbf{Z}^T(t_N) \end{bmatrix}, \quad \mathbf{M}_{rw} = \begin{bmatrix} M_{rw}(t_1) \\ M_{rw}(t_2) \\ \vdots \\ M_{rw}(t_N) \end{bmatrix}. \quad (45)$$

One of the IV method steps consists in building an instrument that is uncorrelated with the noise components. The best instrument is the one that, while respecting the uncorrelatedness with the noise \mathbf{v} , is as much correlated as possible with the original regressor $\boldsymbol{\psi}^T$. Ideally, the optimal instrument is the noise-free version of the regressor $\boldsymbol{\psi}^T$. There are two common choices for the instrument (e.g. [13]): the first consists in using a delayed version of the regressor as instrument, the second uses an ‘‘auxiliary model’’ (together with an input signal) to generate noise-free state estimate from which an estimated noise-free regressor is built and used as instrument.

However, by solving (44), even with an ideal optimal instrument, we would be able to guarantee only consistency of the estimates, while the variance could be still large (this approach is called simple IV method). Optimal IV methods (optimal in the sense of minimum variance) have been studied for several years, considering open-loop linear systems (e.g. [15], [13]), closed-loop linear systems (e.g. [17], [18], [19]), as well as continuous-time systems (e.g. [20], [21]). From these studies, optimal filters have been identified in order to guarantee minimum variance. A detailed description of the general optimal IV method and its relative proof is out of the scope of this paper, and the reader may refer to the previously cited works. The main result from these studies that will be later used is the following:

given a Box-Jenkins model

$$y(t_k) = \frac{B(s)}{A(s)}u(t_k) + \frac{D(s)}{C(s)}e(t_k), \quad (46)$$

the optimal prefilter is

$$F_{opt} = \frac{1}{A(s)} \frac{C(s)}{D(s)}, \quad (47)$$

where $u(t)$, $y(t)$, $e(t)$ are the input, the output and a white noise, respectively, while $A(s)$, $B(s)$, $C(s)$, $D(s)$ represent polynomials¹ characterizing the system model structure ($A(s)$, $B(s)$) and the noise model structure ($C(s)$, $D(s)$). The filter is then applied to the model (regressor, instrument, and ‘‘input’’) and the solution has the same form as (44)

$$\hat{\boldsymbol{\theta}}_{IV} = (\mathbf{Z}_f \boldsymbol{\psi}_f^T)^{-1} (\mathbf{Z}_f \mathbf{M}_{rw_f}). \quad (48)$$

Even if there are no optimal filters for nonlinear systems, if the parameters appear linearly, the IV approach can still be applied and achieve good performance, as shown in [22] where the authors used an IV method for industrial robot model identification.

¹ In this model, s represents the differential operator.

3.3.2 IV Implementation for Satellite Inertia Estimate

Building the instrument

In this work, the instrument is built from estimated (noise-free) states. We assume that the satellite controller is known, as well as the actuator dynamics, and that the reference signals r_1 and r_2 (representing the reference path and feedforward, as shown in Figure 1) are available. The instrument is built as follows:

1. From an "initial" knowledge of the inertia, the satellite dynamic model is built (considered as a rigid body). Then, since the controller and actuator are known, a full closed-loop auxiliary model can be built (as shown in Figure 2);
2. The closed-loop auxiliary model is simulated by using the reference signals as input (r_1 and r_2), and an estimate of the noise-free quaternion $\hat{q}(t)$ is generated, as well as their derivatives $\dot{\hat{q}}(t)$, $\ddot{\hat{q}}(t)$;
3. The instrument is built as $Z^T(t) = \psi^T(\hat{q}(t), \dot{\hat{q}}(t), \ddot{\hat{q}}(t))$.

Since this instrument is built from noise-free reference signal, it is theoretically uncorrelated with the noise term $v(t)$, while the use of the same reference as the real system ensures a high correlation with the regressor $\psi^T(\bar{q}(t), \dot{\bar{q}}(t), \ddot{\bar{q}}(t))$. Generating the noise free-signals from the reaction wheel output, using an open-loop model (Figure 3), would have been not optimal, since the presence of the disturbance $M_d(t)$ would have generated a drift on the estimated $\hat{q}(t)$ and $\dot{\hat{q}}(t)$. Theoretically, the use of the closed-loop auxiliary model can be additionally justified since the feedback signal correlates the input signal (in this case the reaction wheel generated torque) with the noise (e.g. [17]), however, in this scenario since an EKF is present in the feedback, the effect of the noise reaches the output quaternions very attenuated and has therefore a negligible effect on the regressor. It should be noted that even if the actuator dynamics is not perfectly modeled, the generated instrument will still respect the two properties (42) therefore consistent estimates will be guaranteed (there will be instead a slight increase in the variance).

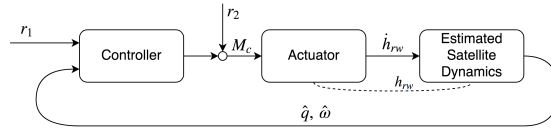


Fig. 2: Closed-loop auxiliary model.

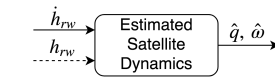


Fig. 3: Open-loop auxiliary model.

Sub-optimal Filtering

As shown in (39), the system is nonlinear, and the IV theory does not provide any solution in order to obtain an optimal filter for the estimation. However, by linearizing the model, a sub-optimal filter can be estimated. The system (39) can be seen

as

$$g(y(t), \dot{y}(t), u(t)) = f(u(t), \dot{u}(t), \ddot{u}(t), \theta) + v(t) + M_d(t), \quad (49)$$

where $u(t)$ represents the state $q(t)$, and $y(t)$ represents the input $h_{rw}(t)$. Model (49) is written as in (46), and some considerations can be made. Firstly, the function f does not have any integrator term, but only derivatives, therefore, even after linearization, it will have no effect on the filter choice ($A(s) = 1$). Secondly, the linearization of the noise components $v(t)$ and the term $M_d(t)$ will give us the information to build a sub-optimal filter.

Let's consider first the case with no disturbance torque $M_d(t)$. As shown in (34-36), the noise term $v(t)$ is function of the inertia parameters θ , and of $h_{rw}(t)$ and $\omega(t)$. By linearizing the system around h_{rw_0} and ω_0 (and using a previous estimate of θ) a first approximation of $\frac{D(s)}{C(s)}$ can be obtained. Since the noise is not affected by the sign, the linearization point has been chosen as the average of the absolute value of h_{rw} and $\bar{\omega}$

$$h_{rw_0} = \frac{1}{N} \sum_{k=1}^N |h_{rw}(t_k)|, \quad \omega_0 = \frac{1}{N} \sum_{k=1}^N |\bar{\omega}(t_k)|. \quad (50)$$

Since the system is multiple-input and multiple-output (MIMO), the following type of linearized noise model is first obtained

$$D_L(s) = \begin{bmatrix} a_{11} & a_{12} & a_{13} \\ a_{21} & a_{22} & a_{23} \\ a_{31} & a_{32} & a_{33} \end{bmatrix} s + \begin{bmatrix} b_{11} & b_{12} & b_{13} \\ b_{21} & b_{22} & b_{23} \\ b_{31} & b_{32} & b_{33} \end{bmatrix} s^2, \quad C_L(s) = 1, \quad (51)$$

where we kept a continuous-time notation. To further simplify (51), the matrices have been diagonalized, replacing the diagonal terms with

$$a_i = \sqrt{a_{i1}^2 + a_{i2}^2 + a_{i3}^2}, \quad b_i = \sqrt{b_{i1}^2 + b_{i2}^2 + b_{i3}^2} \quad \text{for } i = 1 : 3, \quad (52)$$

and therefore $D(s)$ becomes

$$D_L(s) = \begin{bmatrix} a_1 & 0 & 0 \\ 0 & a_2 & 0 \\ 0 & 0 & a_3 \end{bmatrix} s + \begin{bmatrix} b_1 & 0 & 0 \\ 0 & b_2 & 0 \\ 0 & 0 & b_3 \end{bmatrix} s^2. \quad (53)$$

Finally, an additional simplification is performed: since the term a_i (as well as b_i) are very close to each other, the average of a_i and of b_i is used for all the three dimensions, obtaining three identical scalar noise models

$$D_L(s) = a \cdot s + b \cdot s^2. \quad (54)$$

Given this linearized noise model and from (47), the sub-optimal filter for each input and regressor component would have therefore the following form

$$F_{s_{opt}}(s) = \frac{C_L(s)}{D_L(s)} = \frac{1}{bs^2 + as}. \quad (55)$$

This filter has very high performance in the disturbance free case, however it will underperform (will achieve higher variance) if disturbances are present since the filter (55) will integrate M_d .

In order to take into account the disturbance in the filter choice, the disturbance torque must be modeled. We approximated the disturbance as a filtered random walk

$$\dot{M}_d = -\gamma M_d + \eta \quad \text{where} \quad \eta_x \sim \eta_y \sim \eta_z \sim N(0, \sigma_\eta). \quad (56)$$

where γ is an empirical value (e.g. $\gamma = 0.002s^{-1}$) that considers the very low-pass behavior of the main disturbance components. Alternatively, the disturbance torque could be modeled by a simpler integral random walk noise $\dot{M}_d = \eta$, like in [7].

The noise term including the disturbance can be then approximated as

$$v_x = (bs^2 + as)e_x + \frac{1}{s + \gamma}\eta_x. \quad (57)$$

In order to “merge” the terms, the ratio between σ_e and σ_η must be computed. The value of σ_e can be easily obtained from the sensor datasheet, while for σ_η , a rough estimate can be obtained from the knowledge of the typical disturbance torque magnitude. The overall noise transfer function can be then written as

$$bs^2 + as + \frac{\sigma_\eta/\sigma_e}{s + \gamma}, \quad (58)$$

and the filter takes the form

$$F_{s_{opt}}(s) = \frac{s + \gamma}{c_3s^3 + c_2s^2 + c_1s + c_0} \quad (59)$$

Iterative IV algorithm

The overall IV algorithm can be summarized as follows

1. apply the smoothing filter to the quaternion measurements $\bar{q}(t)$ and compute their time derivatives ($\dot{\bar{q}}(t), \ddot{\bar{q}}(t)$);
2. apply the least squares method to obtain a first inertia parameter estimate θ_0 (an additional low-pass second order filter can be applied to improve this initial estimate);
3. update the auxiliary model and the filter $F_{s_{opt}}(s)$ with the new inertia values;
4. generate the noise-free quaternion estimates $\hat{q}(t)$ (and their derivatives) from the closed-loop auxiliary model and the reference signals $r_1(t)$ and $r_2(t)$;
5. build the instrument from $\hat{q}(t)$, $\dot{\hat{q}}(t)$ and $\ddot{\hat{q}}(t)$;
6. filter the regressor, the instrument and the input vector ($M_{rw}(t)$) with the filter $F_{s_{opt}}(s)$, obtaining

$$\psi_f^T(t), \quad Z_f^T(t), \quad M_{rw_f}(t); \quad (60)$$

7. estimate the inertia with the IV method

$$\hat{\theta}_{IV} = \left[\sum_{k=1}^N Z_f(t_k) \psi_f^T(t_k) \right]^{-1} \left[\sum_{k=1}^N Z_f(t_k) M_{rwf}(t_k) \right], \quad (61)$$

Repeat steps 3-4-5-6-7 until $\hat{\theta}_{IV}$ reaches convergence (usually the convergence is reached in 3 iterations).

Augmented regressor and instrument

We mentioned that the overall noise term v , depending on the star tracker orientation and noise standard deviation, may have non-zero expected value. In order to prevent biased estimates for this condition, the regressor and instrument can be augmented [12]

$$\psi_{aug}^T(t_k) = [\psi^T(t_k), I_3], \quad Z_{aug}^T(t_k) = [Z^T(t_k), I_3] \quad \forall k \in [1 \dots N], \quad (62)$$

where $I_3 \in \mathbb{R}^{3 \times 3}$ is the identity matrix. The parameter vector estimate θ_{aug} will contain the 6 inertia parameters, as well the 3 additional bias estimate. This augmented approach will also estimate possible constant components of the disturbance torque $M_d(t)$.

In the satellite scenario, the obtained filter (48) has a very slow dynamics, therefore the initial conditions of the filter have a significant impact on the inertia estimates. Waiting for the end of the transient behavior may results in discarding a significant portion of the data, therefore an alternative solution consists in estimating the filter initial condition together with the inertia parameters. The solution consists in augmenting the regressor and instrument, similarly to (62):

$$\begin{aligned} \psi_{aug}^T(t_k) &= [\psi^T(t_k), T_{r1}(t_k) \ T_{r2}(t_k) \ T_{r3}(t_k)], \\ Z_{aug}^T(t_k) &= [Z^T(t_k), T_{r1}(t_k) \ T_{r2}(t_k) \ T_{r3}(t_k)], \end{aligned} \quad (63)$$

where $T_{ri}(t_k)$ are the transient behaviors corresponding to each one of the 3 filter poles.

4 Simulation Results

The proposed estimation method has been tested through numerical simulations. The Microcarb gyroless satellite, from the Myriade class, is considered as spacecraft. In order to generate the data, a high fidelity simulator from CNES² has been used. The main parameters of the simulators are shown hereafter. The nominal satellite inertia matrix is

² French Space Agency.

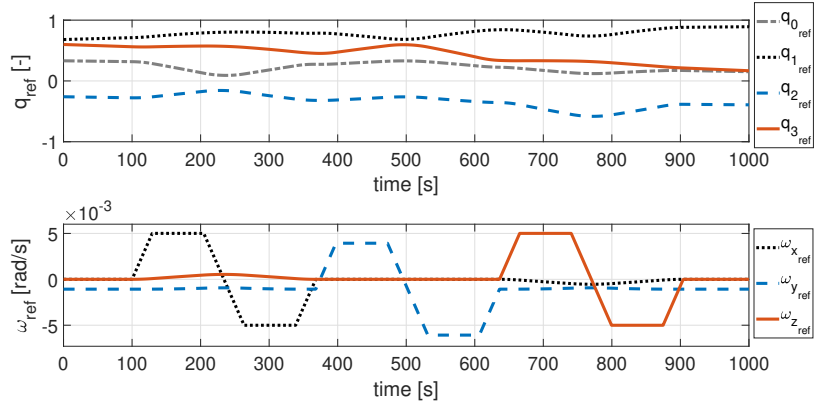


Fig. 4: Attitude and angular rate reference profile.

$$J_0 = \begin{bmatrix} 20.3852 & -3.7497 & -1.7515 \\ -3.7497 & 24.5764 & 0.7836 \\ -1.7515 & 0.7836 & 29.0328 \end{bmatrix} [kgm^2]. \quad (64)$$

The satellite is controlled by four reaction wheels. Since we assumed that the actuator alignments are known as well as their inertia, and that the noise on the reaction wheel speeds is negligible, we have direct access to the reaction wheel angular momentum h_{rw} . All the sensor sampling frequencies are set to $4Hz$. The noise standard deviation on the star tracker was set as $\sigma_x = \sigma_y = 11.7 \cdot 10^{-6} rad$ and $\sigma_z = 93 \cdot 10^{-6} rad$. The star tracker model had also bias and harmonic (at the orbital frequency) noise terms: the bias was set to $b_x = b_y = 58 \cdot 10^{-6} rad$, $b_z = 53 \cdot 10^{-6} rad$, while the harmonic amplitude was $\alpha_x = \alpha_y = 8 \cdot 10^{-6} rad$, $\alpha_z = 23 \cdot 10^{-6} rad$ (both in the star tracker frame). All the main types of disturbance torques are considered³: aerodynamic torque, solar radiation pressure, magnetic torque, gravity gradient torque, as well as internal oscillation in the structure (mainly due to flexible elements like solar panels). Additionally, the satellite is equipped with a scanning mirror, that is generating additional disturbances. During the simulations, the solar panel are kept fixed in order to avoid any change of the satellite inertia during the estimation. The control law is described in (1) and (2). The reference guidance profile is shown in Figure 4, and it is kept the same for every simulation. Figure 5 shows the input-output of the satellite for a single simulation.

Two types of Monte Carlo simulations are performed: the first one consists in having a star tracker following the simple model (16), while the second considers a more realistic case, where also bias and harmonic noise terms are considered. In order to have a different disturbance torque profile, the initial satellite orbit position

³ The satellite is operating in low Earth orbit (LEO).

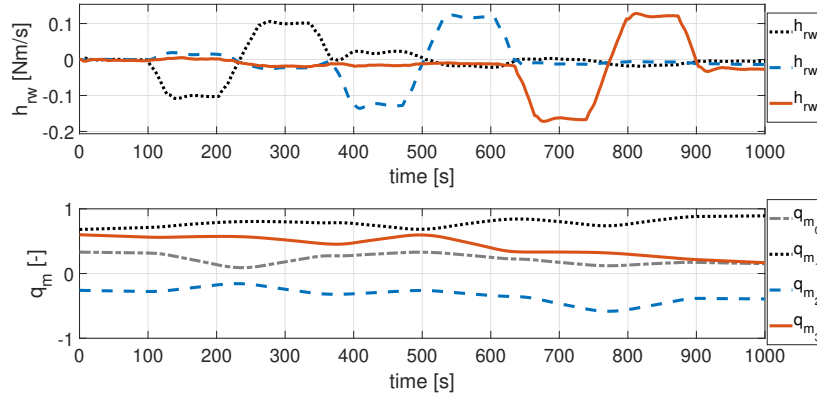


Fig. 5: Input (reaction wheel total angular momentum) and output (in quaternions) of the satellite.

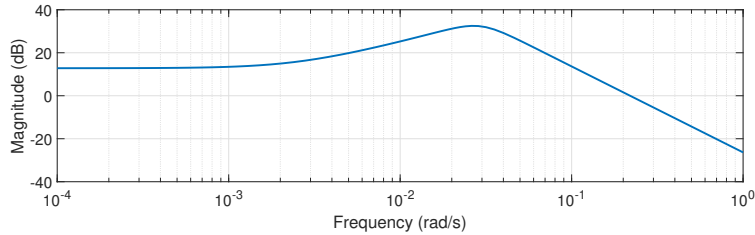


Fig. 6: Magnitude Bode plot of the filter used in the IV method.

is different in every simulation. A typical magnitude Bode plot of the filter used by the IV method is shown in Figure 6.

Table 1 shows the results from a Monte Carlo simulation of 100 runs. In both cases the estimates present a low variance and a slight bias, however, the presence of bias in the quaternions does not seem to have a significant impact in the performance. The slight bias is mainly due to the disturbance torque, while, even in the biased star tracker case, the correlation between the noise term e and the noise free quaternions q is too small to generate any significant change (as shown in the comparison of Table 1). The table includes also the results from a least squares algorithm with a second-order low pass filter, used as comparison, which shows a considerably higher variance.

The main user-parameter to be set is the ratio between σ_η and σ_e . Figure 7 shows the mean square errors of the inertia estimates for different ratios, in order to demonstrate the algorithm robustness.

	$J_{11} [kg m^2]$		$J_{22} [kg m^2]$		$J_{33} [kg m^2]$		$J_{23} [kg m^2]$		$J_{13} [kg m^2]$		$J_{12} [kg m^2]$	
	mean	st.d.										
$\hat{\theta}_{LS}$	20.431	0.034	24.687	0.033	29.021	0.036	0.766	0.033	-1.742	0.031	-3.783	0.041
$\hat{\theta}_{N_1}$	20.397	0.006	24.625	0.008	29.054	0.008	0.776	0.011	-1.742	0.009	-3.743	0.005
$\hat{\theta}_{N_2}$	20.397	0.006	24.625	0.008	29.055	0.008	0.776	0.010	-1.741	0.009	-3.743	0.005
θ_0	20.385		24.576		29.033		0.784		-1.751		-3.768	

Table 1: Results from a Monte Carlo simulation of 100 runs using different satellite starting orbit positions. The true value is represented by θ_0 . θ_{N_1} is the inertia estimate for the unbiased star tracker, whereas θ_{N_2} is for the biased case. In this simulation settings, the performance difference is negligible. Additionally, θ_{LS} shows the results from a least squares method with a second order low-pass filter.

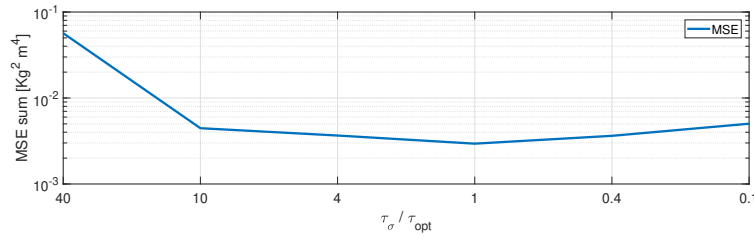


Fig. 7: Sum of the mean square errors (MSE) of the 6 inertia parameter estimates for different values of the user-parameter τ_σ . The value of τ_σ is represented as its ratio with an empirical optimal value τ_{opt} .

5 Conclusions

A satellite inertia parameter estimator based on an IV approach has been implemented. Unlike common inertia estimators, the proposed iterative IV method does not require gyroscope measurements and it can just rely on attitude sensors. A semi-adaptive filter for the IV method has been proposed, that takes into account both the sensor noise and the disturbance torque in order to achieve close to minimum variance. The overall method removes some of the theoretical limitations of the least squares method, while, thanks to its convex cost function, it is robust with respect to the initial conditions, and also with respect to the main user-parameter (σ_η / σ_e). The overall algorithm performance has been demonstrated via Monte Carlo simulations, using data generated by a high-fidelity simulator provided by CNES. Additional works will consider the estimation of the actuator alignments, improvement of the disturbance rejection, online implementation of the algorithm, and the choice of optimal maneuvers in order to improve the information content of the data.

References

1. A. Y. Lee and J. A. Wertz, "In-flight estimation of the Cassini spacecraft's inertia tensor," *Journal of spacecraft and rockets*, vol. 39, no. 1, pp. 153–155, 2002.
2. M. C. Norman, M. A. Peck, and D. J. O'shaughnessy, "In-orbit estimation of inertia and momentum-actuator alignment parameters," *Journal of Guidance, Control and Dynamics*, vol. 34, no. 6, pp. 1798–1814, 2011.
3. M. C. VanDyke, J. L. Schwartz, and C. D. Hall, "Unscented Kalman filtering for spacecraft attitude state and parameter estimation," *Advances in the Astronautical Sciences*, vol. 118, no. 1, pp. 217–228, 2004.
4. Z. R. Manchester and M. A. Peck, "Recursive inertia estimation with semidefinite programming," in *AIAA Guidance, Navigation, and Control Conference*, p. 1902, 2017.
5. M. L. Psiaki, "Estimation of a spacecraft's attitude dynamics parameters by using flight data," *Journal of Guidance Control and Dynamics*, vol. 28, no. 4, p. 594, 2005.
6. M. Thoby, "Myriade: Cnes micro-satellite program," 2001.
7. H. Yoon, K. M. Riesing, and K. Cahoy, "Kalman filtering for attitude and parameter estimation of nanosatellites without gyroscopes," *Journal of Guidance, Control, and Dynamics*, vol. 40, no. 9, pp. 2272–2288, 2017.
8. J. L. Crassidis, F. L. Markley, and Y. Cheng, "Survey of nonlinear attitude estimation methods," *Journal of guidance, control, and dynamics*, vol. 30, no. 1, pp. 12–28, 2007.
9. F. Genin and F. Viaud, "An innovative control law for Microcarb microsatellite," *32nd annual AAS Guidance and Control Conference*, 2018.
10. M. J. Sidi, *Spacecraft dynamics and control: a practical engineering approach*, vol. 7. Cambridge university press, 1997.
11. J. Diebel, "Representing attitude: Euler angles, unit quaternions, and rotation vectors," *Matrix*, vol. 58, no. 15-16, pp. 1–35, 2006.
12. B.-E. Jun, D. S. Bernstein, and N. H. McClamroch, "Identification of the inertia matrix of a rotating body based on errors-in-variables models," *International Journal of Adaptive Control and Signal Processing*, vol. 24, no. 3, pp. 203–210, 2010.
13. T. Söderström and P. Stoica, *Instrumental variable methods for system identification, Lectures Notes in Control and Information Sciences*. Springer-Verlag, Berlin, 1983.
14. L. Ljung, *System identification: Theory for the user*. Prentice-Hall, 2nd ed., 1999.
15. P. C. Young, *Recursive estimation and time-series analysis: An introduction for the student and practitioner*. Springer, 2nd ed., 2011.
16. C. Nainer, H. Garnier, M. Gilson, and C. Pittet, "In-orbit data driven identification of satellite inertia matrix," *18th IFAC Symposium on System Identification (SYSID)*, 2018.
17. P. Van den Hof, "Closed-loop issues in system identification," *Annual reviews in control*, vol. 22, pp. 173–186, 1998.
18. M. Gilson and P. Van den Hof, "Instrumental variable methods for closed-loop system identification," *Automatica*, vol. 41, no. 2, pp. 241–249, 2005.
19. M. Gilson, H. Garnier, P. C. Young, and P. M. Van den Hof, "Optimal instrumental variable method for closed-loop identification," *IET control theory & applications*, vol. 5, no. 10, pp. 1147–1154, 2011.
20. F. Chen, H. Garnier, M. Gilson, J. C. Agüero, and T. Liu, "Refined instrumental variable parameter estimation of continuous-time Box–Jenkins models from irregularly sampled data," *IET Control Theory & Applications*, vol. 11, no. 2, pp. 291–300, 2016.
21. H. Garnier, "Direct continuous-time approaches to system identification. overview and benefits for practical applications," *European Journal of Control*, vol. 24, pp. 50–62, 2015.
22. M. Brunot, A. Janot, P. Young, and F. Carrillo, "An improved instrumental variable method for industrial robot model identification," *Control Engineering Practice*, vol. 74, pp. 107–117, 2018.